Dipole-dipole resonance line shapes in a cold Rydberg gas

B. G. Richards and R. R. Jones
Department of Physics, University of Virginia, Charlottesville, Virginia 22904-4714, USA
(Received 31 January 2016; published 18 April 2016)

We have explored the dipole-dipole mediated, resonant energy transfer reaction, $32p_{3/2} + 32p_{3/2} \rightarrow 32s + 33s$, in an ensemble of cold ^{85}Rb Rydberg atoms. Stark tuning is employed to measure the population transfer probability as a function of the total electronic energy difference between the initial and final atom-pair states over a range of Rydberg densities, $2 \times 10^8 \leqslant \rho \leqslant 3 \times 10^9$ cm^{-3}. The observed line shapes provide information on the role of beyond nearest-neighbor interactions, the range of Rydberg atom separations, and the electric field inhomogeneity in the sample. The widths of the resonance line shapes increase approximately linearly with the Rydberg density and are only a factor of 2 larger than expected for two-body, nearest-neighbor interactions alone. These results are in agreement with the prediction [B. Sun and F. Robicheaux, Phys. Rev. A **78**, 040701(R) (2008)] that beyond nearest-neighbor exchange interactions should not influence the population transfer process to the degree once thought. At low densities, Gaussian rather than Lorentzian line shapes are observed due to electric field inhomogeneities, allowing us to set an upper limit for the field variation across the Rydberg sample. At higher densities, non-Lorentzian, cusplike line shapes characterized by sharp central peaks and broad wings reflect the random distribution of interatomic distances within the magneto-optical trap (MOT). These line shapes are well reproduced by an analytic expression derived from a nearest-neighbor interaction model and may serve as a useful fingerprint for characterizing the position correlation function for atoms within the MOT.

DOI: 10.1103/PhysRevA.93.042505

I. INTRODUCTION

Because of their large transition dipole moments, Rydberg atoms are greatly affected by weak electric fields, including the multipole fields of neighboring atoms [1]. Accordingly, interactions between Rydberg atoms can be quite strong, coupling electronic and center-of-mass degrees of freedom at large internuclear separations. Rydberg-Rydberg interactions were originally studied in the context of collisions in thermal samples [1]. More recently, however, attention has turned to the exploration and control of the coherent couplings that exist between Rydberg atoms in (nearly) frozen gases, where the thermal kinetic energy of the atoms is less than their mutual interaction energies [2–32]. Such interactions enable a variety of few- and many-body quantum phenomena as well as potential applications in quantum information [5,33–36]. Typically, dipole-dipole (DD) effects dominate the atom-atom interaction when the spacing between the Rydberg atoms is much larger than the radial extent of the electronic wave function on individual atoms.

The degree to which the DD coupling between Rydberg atoms influences their behavior depends sensitively on the energy level structure of the individual atoms. Given their large polarizabilities, it is straightforward to manipulate the interactions between Rydberg atoms by applying static or pulsed electric fields. Stark-tuned, (Förster) resonant energy transfer (RET) reactions have been studied in both thermal [1,37,38] and cold Rydberg gases [3,4,6,8,9,12–14,16,17,22,29,31], and are perhaps the simplest example of electric-field controlled DD interactions involving Rydberg atoms. As an example of a RET process, consider two identical atoms A and B, separated by a distance R and initially in the same Rydberg state $|P\rangle$. Direct electronic energy transfer from A to B can efficiently occur, with little or no center-of-mass translational energy exchange, if there exist two states, $|S\rangle$ and $|S'\rangle$, with energies $E_{S,P} \simeq -E_{S',P}$ relative to $|P\rangle$. Assuming $|S\rangle$, $|P\rangle$, and $|S'\rangle$ are adjacent Rydberg levels with approximately the same principal quantum number n, the transition matrix elements $\mu_A = \langle S|r_A|P\rangle$ and $\mu_B = \langle S'|r_B|P\rangle$ are large (scaling as n^2) and energy transfer from A to B is facilitated by a DD-interaction $V_{dd} \sim \mu_A\mu_B/R^3$ (atomic units are used unless otherwise noted) [1]. Here, r_A and r_B are the distances between the electron and nucleus on atoms A and B, respectively. The energy transfer results in the excitation of atom B from $|P\rangle$ to $|S'\rangle$ and simultaneous deexcitation of atom A from $|P\rangle$ to $|S\rangle$. The process is resonant, and most efficient, when the applied field is tuned to a value $F = F_0$ where the detuning $\delta = E_{S,P} + E_{S',P} = 0$.

In the context of collisions it makes sense to discuss the DD interaction between a pair of atoms in terms of RET between the individual atoms. However, in a frozen gas, the DD interaction between two atoms is more conveniently discussed as a coherent coupling between molecular, or atom-pair states. For the example in the preceding paragraph, the relevant (uncoupled) pair states at large R are $|P\rangle|P\rangle$ and $|S\rangle|S'\rangle$. At smaller R, the coupled atoms are described by eigenstates which are linear combinations of the two uncoupled pair states. Through the DD interaction, the probability amplitude initially in $|P\rangle|P\rangle$ can be coherently transferred to $|S\rangle|S'\rangle$ (and back) at a rate, and with a maximum probability, that depends on μ_A, μ_B, R, and δ. For samples involving more than two atoms, the coupling between non-nearest-neighbor atoms complicates the eigenstate composition and the coherent population transfer processes. Indeed, measurements of Rydberg population transfer probability, as a function of the detuning δ from DD resonance, have provided evidence that many-body interactions play an important role in the coupled-atom dynamics in large ensembles [3,4]. Also, clear changes in resonance "line shapes" have been observed as the number of interacting atoms increases from 2 to several [22].

Using line shape measurements for the $32p_{3/2}32p_{3/2} \leftrightarrow 32s33s$ DD resonance in Rb, we clarify the respective

roles of nearest- and beyond nearest-neighbor interactions in resonantly coupled systems, and show that the line shapes contain information on the position correlation function of Rydberg atoms in a cold random ensemble.

II. EXPERIMENTAL PROCEDURE

In the experiments, ^{85}Rb atoms at $\sim$70 μK in a magneto-optical trap (MOT) are photoexcited from the $5p_{3/2}$ upper trap state directly to the $32p_{3/2}$ Rydberg state in the presence of a weak electric field, $F \simeq 15$ V/cm. The field mixes a small amount of ns character into the p state to enable the excitation, but detunes the atoms sufficiently far from DD resonance so that, initially, there is negligible interaction between them. The atoms are then exposed to a fast-rising "tuning" electric field pulse. The tuning pulse alters the energy difference δ between the $32p_{3/2}32p_{3/2}$ and $32s33s$ pair states, and projects the initial $32p$ population onto the coupled pair states. The system is allowed to evolve throughout the duration τ of the tuning pulse. State-selective field ionization (SSFI) is then employed to measure the population transferred to $32s33s$ pairs as a function of the tuning field strength and Rydberg density [1].

A 482 nm laser pulse directly excites atoms from the $5p_{3/2}$ trap state to the $32p_{3/2}$ Rydberg state. The experiments are performed using either a "long," narrow-band ($\sim$1 MHz) or "short," broader-band ($\sim$100 MHz) Rydberg excitation pulse. For the long pulse, an acousto-optic modulator (AOM) chops a 3 μs excitation pulse, with $\sim$1 μs rise and fall times, from a narrow band ($\sim$1 MHz) continuous wave diode laser. Alternatively, a Pockels cell is employed to slice a short 10 ns pulse from the diode laser, and that pulse is amplified in dye using the 10 ns, 355 nm third harmonic of a pulsed Nd:yttrium-aluminum-garnet (YAG) laser. In both cases, the 482 nm beam is focused into the 0.4 mm diameter MOT using a 350 mm focal length lens, exciting a cylindrical atomic volume with a diameter of $\sim$0.1 mm and a length of 0.4 mm.

The laser excitation, energy tuning, and field ionization of the Rydberg atoms are facilitated by the application of pulsed and static voltages to two pairs of thin, parallel, stainless steel rods that are arranged around the cold atom cloud in a rectangular array. The field produced by the rods at the position of the MOT is proportional to the voltage difference between rod pairs and is quite uniform, with a variation of 0.07% over the atom cloud. The voltage pulse which produces the tuning field has fast (2 ns) rise and fall times and is produced using an arbitrary wave-form generator (AWG) followed by a DC-coupled, pulse amplifier.

At the end of the interaction period defined by the tuning pulse, a high-voltage ramp applied to the field rods ionizes Rydberg atoms in the interaction region, propelling them toward a microchannel plate (MCP) detector. Different Rydberg states ionize at different times during the ramp [1]. Therefore, in principle, populations in different states can be distinguished in the time-dependent signal from the MCP detector. In practice, to obtain better temporal separation between the signals corresponding to the populations in the initial ($32p_{3/2}32p_{3/2}$) and final ($32s33s$) pair states, the maximum ionization field is set just above the threshold for ionizing $32p_{3/2}$. As a result, we do not ionize atoms in $32s$, and detect only half of the atoms (those in $33s$) in each $32s33s$ pair.

By recording the population transfer to $33s$ as a function of the tuning field, we obtain the resonance line shape (see Fig. 1). Line shapes are measured over a range of Rydberg densities, $2 \times 10^8 < \rho < 3 \times 10^9$ cm^{-3}. The density is varied by adjusting the current applied to the getters that supply Rb to the MOT. The density of atoms in the MOT is determined, to within 30%, by combining measurements of the spatial dimensions of the atom cloud size via direct imaging with a CCD camera with measurements of the radiated fluorescence using an optical power meter [39]. By saturating the Rydberg excitation using a sufficiently high laser fluence, we ensure that approximately one-third of the atoms in the excitation volume are excited to Rydberg states. Data collected as a function of tuning pulse duration τ at a fixed tuning field showed little or no change in the population transfer for $\tau > 1$ μs. Full line shapes were measured over a range of densities for $\tau = 5$ and 15 μs, with no apparent differences in the observed resonance profiles.

In addition to the field produced by the rods, an additional parallel "offset" field of 2.6 V/cm contributes to the net electric field in the interaction region. The offset field is the result of imperfect shielding of the MCP detector and is less homogeneous than the rod field. As discussed in more detail below, the measured line shapes can be used to characterize the variation in this offset field over the atomic ensemble.

III. EXPERIMENTAL RESULTS

Figure 1 shows the population transferred to $33s$ as a function of the strength of the applied tuning field at three different densities. These line shape data exhibit several notable features. First, the functional form of the resonance lines change from something resembling a Gaussian at low density to a cusp, characterized by a narrow central peak with broad wings, at higher density. As described in detail in the next section, the cusp line shape reflects the random variation in the interatomic spacing R within the random ensemble.

Second, the maxima of the three line shapes appear at (slightly) different applied tuning fields, at values closer to 10.1 V/cm than to the expected value, $F_0 = 12.7$ V/cm, at which the resonance condition, $\delta = 0$, is fulfilled for atoms initially in the $32p_{3/2}$ $|m_j| = 3/2$ state. Here m_j is the projection of total electronic angular momentum on the z-axis. As noted previously, the nominal 2.6 V/cm MCP offset field adds to the applied field from the rods, shifting the apparent resonance field. The variation in the peak position for different data sets is not caused by the different densities at which the data were taken, but is due rather to the inhomogeneity in the offset field and slight differences in the position of the Rydberg excitation laser within the MOT for different data runs. The spatial variation in the offset field within the Rydberg excitation beam is responsible for the Gaussian, inhomogeneously broadened line shapes observed at low density.

Third, the widths of the line shapes grow linearly with increasing density. Figure 2 shows the full width at half maximum (FWHM), Δ, of the measured resonance profiles as a function of Rydberg density. To convert the resonance widths (which are measured in units of field) to units of energy, we first measure the Stark shifts of the $32p_{3/2}$, $32s$, and $33s$ states

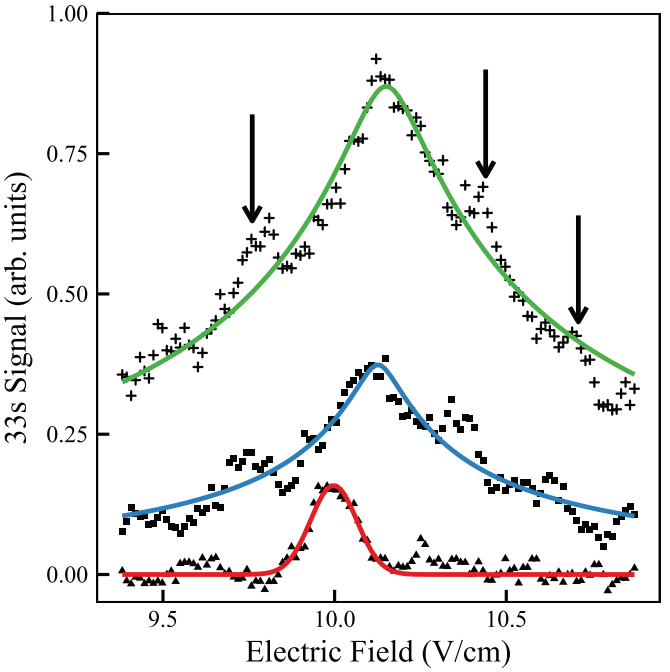

FIG. 1. $32p_{3/2}32p_{3/2} \rightarrow 32s33s$ DD-resonance line shapes, showing population transfer to $33s$ as a function of applied tuning field at various Rydberg densities: $\rho = 2 \times 10^8$ (filled triangles); $\rho = 1 \times 10^9$ (filled squares); and $\rho = 3 \times 10^9$ cm^{-3} (crosses). The measured signals are not individually normalized, so the relative heights of the profiles reflects the difference in resonant transition probability. The baseline, corresponding to zero population transfer, is the same for the three data sets. The horizontal axis shows the applied tuning field due to the rods. The resonance line centers are shifted from the expected resonance condition, $F_0 = 12.7$ V/cm, due to the presence of the MCP offset field described in the text. The three data sets are acquired with the excitation beam focused at (slightly) different locations within the MOT. The relative shifts of the line centers are due to the variation in the offset field within the FWHM of the atom cloud. As described in the text, the inhomogeneity in the offset field is also responsible for the Gaussian line shapes observed at low Rydberg density. The solid (red) line through the lowest density data is the best Gaussian fit of the inhomogeneously broadened line shape. The solid (blue and green) lines through the higher density data are fits to the cusp line shape expected for a random ensemble, as described in the text. The small peaks indicated by arrows on either side of the resonance data appear independent of density. The two features on the high-field side of the resonance can be attributed to the transfer of population to $31d$ (not resolved from $33s$ in the ionization signal) due to $32p_{3/2} + 32p_{3/2} \rightarrow 31d + 29k$ resonances, where the $29k$ states are members of the manifold of $n = 29$ Stark states that adiabatically connect to high-ℓ states in zero field. The specific resonance(s) responsible for the feature(s) on the low field side of the primary resonance have not been identified.

as a function of applied field in the vicinity of the resonance. We then use those spectroscopic data to compute the detuning δ as a function of the applied field (see Fig. 3). We find that near F_0, δ varies approximately linearly with F with a slope of 170 MHz/(V/cm). Note that since the tuning field, not the excitation laser, determines the detuning of the atoms from resonance, the laser bandwidth does not factor into the measured resonance widths.

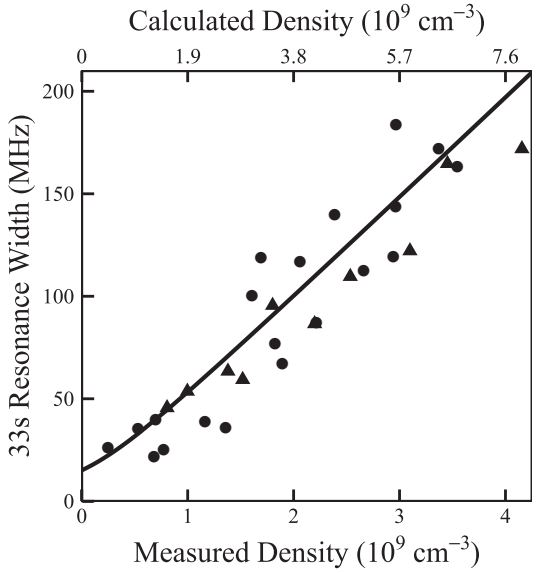

FIG. 2. Resonance width as a function of Rydberg density. Measured widths are shown as points (lower density axis) while the solid line shows the calculated widths (upper density axis) assuming only nearest-neighbor interactions and 15 MHz of inhomogeneous broadening due to the offset field. The filled circles show data taken with a long 3 μs excitation laser pulse, and the filled triangles show data taken with a short 10 ns excitation pulse. No significant difference in the profile widths for the long and short pulse excitations is expected or observed.

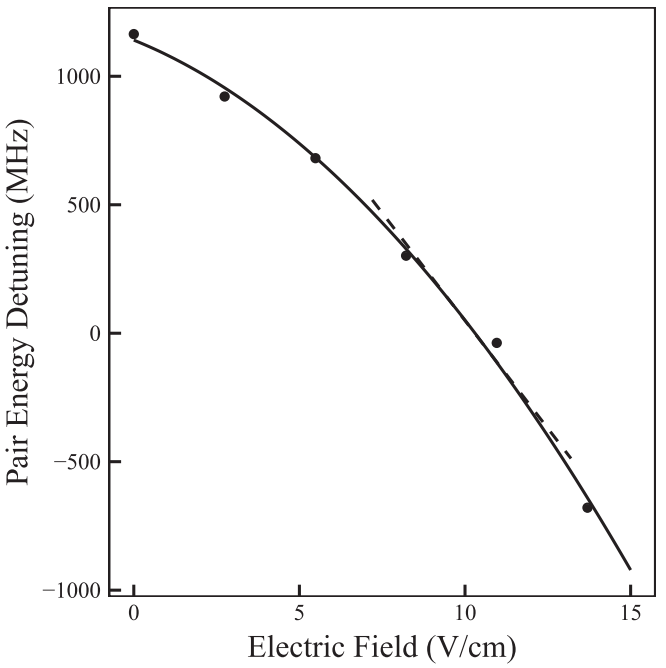

FIG. 3. Pair-energy detuning from resonance as a function of applied electric field. The filled circles are experimentally determined values of δ obtained from Stark shift measurements for the $32p_{3/2}$ $|m_j| = 3/2$, $32s$, and $33s$ levels as a function of the applied field. At these low fields, the energies of all three levels shift quadratically with the field. The solid line is a quadratic fit to the data. Near resonance, the variation in δ is approximately linear with a slope of 170 MHz/(V/cm) (dashed line).

IV. ANALYSIS AND DISCUSSION

The resonance line shapes carry information on the relative strength of nearest- and beyond nearest-neighbor interactions, the distribution of atom separations, and field inhomogeneities in the Rydberg ensemble. In order to extract that information we must identify how each of these influences the different features in the observed profiles. To that end, we first consider the form of the line shape associated with a pair of stationary atoms with a well-defined separation, coupled via a (near) resonant $32p32p \leftrightarrow 32s33s$ DD interaction. We diagonalize the Hamiltonian in the presence of the DD interaction, restricting the pair-state basis to those levels which are degenerate at resonance. This basis includes numerous states with different azimuthal quantum numbers m for the individual atoms and different values of total electronic angular momentum and its projection on the internuclear axis [38,39]. However, ignoring spin, there are only two interacting states and the problem reduces to an equivalent two-level system, involving two pair basis states, $|1\rangle$ and $|2\rangle$, with a DD coupling $V_{dd} = \frac{2\mu_A\mu_B}{\sqrt{3}R^3}$ between them. Here $|1\rangle$ is a linear combination of $32p32p$ states, $|2\rangle$ is an equal admixture of $32s33s$ and $33s32s$, and μ_A and μ_B are defined as in the Introduction.

Diagonalizing the effective two-level Hamiltonian, one obtains the eigenstates

$$\begin{aligned} |+\rangle &= \cos\theta|1\rangle + \sin\theta|2\rangle, \\ |-\rangle &= -\sin\theta|1\rangle + \cos\theta|2\rangle, \end{aligned} \tag{1}$$

where $\tan 2\theta = 2V_{dd}/\delta$. These eigenstates have energies $E_\pm = (\delta \pm \Gamma)/2$, where $\Gamma = \sqrt{\delta^2 + 4V_{dd}^2}$, and exhibit a standard avoided level crossing as a function of δ, with an energy separation $\Delta E = E_+ - E_- = 2V_{dd}$ at $\delta = 0$. At large detunings from resonance, $|+\rangle$ and $|-\rangle$ have only p- and s-character, respectively. Thus, the initial laser excitation, which is performed in an electric field for which atom pairs are far-detuned from the $32p32p \leftrightarrow 32s33s$ resonance, creates only $32p$ atoms, thereby populating only $|+\rangle$. At $t = 0$, the fast rising tuning-field pulse then projects the $32p32p$ atom pairs into a coherent superposition of $|+\rangle$ and $|-\rangle$.

Initially, the time-dependent electronic wave function of each atom pair has only $32p32p$ character. However, assuming coherence is maintained, the pair state evolves as a wave packet in the uncoupled basis, according to the two-level Rabi formula:

$$\Psi(t) = [\cos(\Gamma t/2) - i\eta\sin(\Gamma t/2)]|1\rangle + i\chi\sin(\Gamma t/2)|2\rangle, \tag{2}$$

where Γ is the effective Rabi frequency, $\chi = 2V_{dd}/\Gamma$, and $\eta = \delta/\Gamma$ is a scaled detuning.

The principal signature of the evolution of this wave packet is the coherent transfer of population from $|1\rangle$ to $|2\rangle$, i.e., from p- to s-character. According to Eq. (2), the probability of finding an atom in the $33s$ state at a time t following the start of the tuning pulse is, $\mathcal{P}_0 = \chi^2\sin^2(\Gamma t/2)$. The temporal modulations in $\mathcal{P}_0$, predicted for a single atom pair, can be viewed as Rabi oscillations due to the coupling between the pair states $|1\rangle$ and $|2\rangle$ or, alternatively, as a quantum beat induced by the coherent excitation of the DD-dressed states $|+\rangle$ and $|-\rangle$. The amplitude of the Rabi oscillations, χ^2, is a Lorentzian function of the detuning δ centered at $\delta = 0$ with a FWHM, $\Delta = 4V_{dd}$.

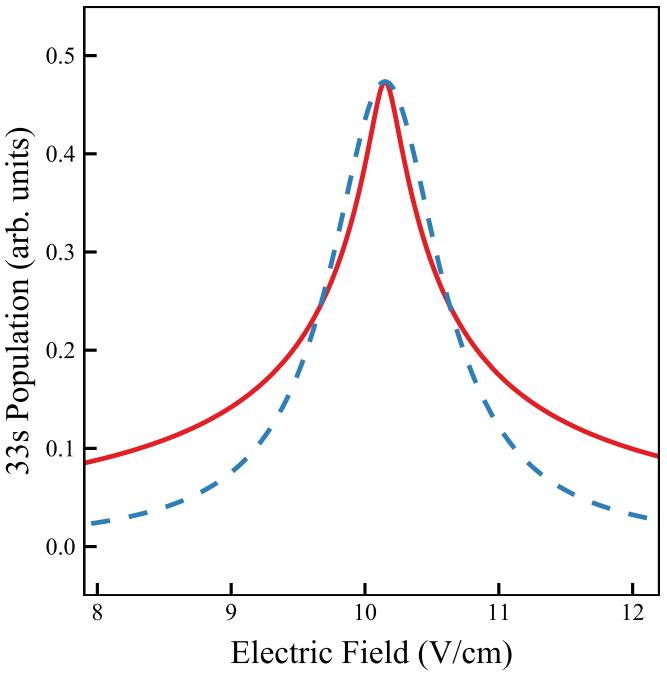

FIG. 4. Comparison of the cusp (solid line) and Lorentzian (dashed line) line shapes expected for ensembles with random [see Eq. (5)] and uniform [see Eq. (3)] atom separation, respectively. The Lorentzian profile assumes the most probable value of R at the Rydberg density used to compute the cusp. Note the cusp's broad, large amplitude wings and relatively narrow central peak.

Experimentally, we measure the number of $33s$ atoms, produced via DD resonance, from a random ensemble of $32p$ atoms. Within the ensemble, there is a broad distribution of atom separations and, therefore, a wide range of values for V_{dd} and Γ for different atom pairs. As a result, a monotonic increase and eventual saturation, but no Rabi oscillations, are actually observed in the $33s$ population measured as a function of the interaction time, τ. Accordingly, for sufficiently long τ, one might expect the ensemble to exhibit a Lorentzian population transfer line shape (see Fig. 4) that is approximately equal to the time-averaged value of $\mathcal{P}_0$ for a single atom pair

$$\mathcal{P} = \frac{1}{2}\chi^2 = \frac{2V_{dd}^2}{\delta^2 + 4V_{dd}^2}, \tag{3}$$

with the values of χ and V_{dd} computed using $R \simeq (2\pi\rho)^{-1/3}$, the most probable nearest-neighbor separation in the ensemble. Assuming only nearest-neighbor interactions, this approximation correctly predicts the FWHM of the resonance, Δ, but it is a poor representation of the line shape overall.

To properly account for the variation in atom separations throughout the excitation volume, we integrate Eq. (3) over all R, weighting the contribution from each R by the nearest-neighbor distribution for a random ensemble [40]

$$P(R) = 4\pi\rho R^2 e^{-\frac{4}{3}\pi\rho R^3}. \tag{4}$$

The line shape resulting from the integration can be expressed in terms of standard functions as

$$\mathcal{P} = \frac{1}{2}a\left\{\mathrm{Ci}(a)\sin a + \left[\frac{\pi}{2} - \mathrm{Si}(a)\right]\cos a\right\}, \qquad (5)$$

where $a = 16\pi\rho\mu_A\mu_B/(3\sqrt{3}\delta)$, $\mathrm{Si}(x) = \int_0^x \frac{\sin u}{u}du$ is the sine integral, $\mathrm{Ci}(x) = \gamma + \ln x + \int_0^x \frac{\cos u - 1}{u}du$ is the cosine integral, and $\gamma \simeq 0.577216$ is Euler's constant [41]. As shown in Fig. 4, the line shape takes the form of a cusp which has a narrower central peak and significantly broader wings as compared to the Lorentzian profile computed at the same Rydberg density, but using a uniform atom separation equal to the most probable value of R. It is worth noting, however, that the FWHM of the two line shapes

$$\Delta \simeq 16\pi\rho\mu_A\mu_B/\sqrt{3} \qquad (6)$$

are identical, and as expected, are directly proportional to the Rydberg density. For the $32p32p \leftrightarrow 32s33s$ resonance, we compute $\mu_A = \langle 32s|r|32p\rangle = 964$ and $\mu_B = \langle 33s|r|32p\rangle = 941$, giving $\Delta = 26$ MHz for $\rho = 1 \times 10^9$ cm^{-3}.

In Fig. 1, the solid curves drawn through the data collected at $\rho = 1 \times 10^9$ and $\rho = 3 \times 10^9$ cm^{-3} are fits of Eq. (5) to those line shapes. The fits capture the primary features of the observed profiles when the weaker satellite resonances in the data are ignored. At these densities, the "natural" width due to the DD interaction is the dominant contributor to the line shape, and inhomogeneous broadening due to the spatial variation in the offset field has a negligible effect. The broad wings of the line shapes distinguish them from the Lorentzians expected for ensembles with well-defined atom separation. Conversely, for $\rho = 2 \times 10^8$ cm^{-3}, the natural width is less than the inhomogeneous width. As a result, in convolution, the measured profile is well represented by a Gaussian with negligible wings far from resonance.

The solid curve in Fig. 2 is the FWHM of a simulated profile that is constructed by convoluting the cusp of Eq. (5), whose natural width increases proportionally to the Rydberg density, with a fixed-width (15 MHz) Gaussian. The Gaussian is included to model the effects of inhomogeneous broadening associated with the spatial variation in the applied electric field, and its FWHM is chosen to be in accord with the resonance widths measured at the lowest densities. In the following, we argue that the principal source of the observed inhomogeneous broadening is the gradient in the offset field produced by the MCP. As noted previously, the variation in the rod field over the interaction region is only 0.07%, leading to a variation in δ of approximately 1 MHz for tuning fields near the resonance condition. While there is a magnetic field gradient in the interaction region due to the MOT coils, the variation in δ due to Zeeman shifts is also ~1 MHz. Both of these inhomogeneities are essentially negligible when taken in quadrature with the other sources of broadening that lead to the combined 15 MHz inhomogeneous width observed at very low density. Given the detuning slope of 170 MHz/(V/cm) near resonance, an offset field variation of 0.085 V/cm accounts for the 15 MHz minimum width. Interestingly, a very similar offset field variation, 0.081 V/cm, when taken in quadrature with magnetic field inhomogeneity, also explains the 4.2 MHz minimum width observed in independent measurements of the $25s33s \leftrightarrow 24p34p$ resonance, using the same apparatus and experimental geometry [29]. The latter resonance has considerably different tuning properties, including a detuning slope of 51 MHz/(V/cm) and resonant field of 3.4 V/cm, making it highly unlikely that the agreement between the two field variation determinations is coincidental.

The overlap of the simulated and measured line widths in Fig. 2 is accomplished by doubling the natural width predicted by Eq. (6) for the cusps used in the simulations. In the figure, we represent that doubling by displaying the calculated and measured widths on density scales that differ by approximately a factor of 2. This illustrates that the discrepancy could be the result of an underestimate of the measured Rydberg density. That said, given the 30% estimated density uncertainty, it is unlikely that the factor of 2 is due to the density calibration alone.

Another potential source of broadening is relative atom motion which is neglected in our model. For $\rho = 2 \times 10^9$ cm^{-3}, the most probable atom separation is $R \sim 4$ μm and the rms relative velocity between two 70 μK atoms is $v_{rms} = 0.2\mu\mathrm{m}/\mu\mathrm{s}$. Depending on the direction of relative motion, in a $\tau = 10$ μs interval, the separation between typical nearest neighbors changes by 10 to 50% due to their thermal motion. Despite this motion, within the data spread shown in Fig. 2, we find the same resonance widths for tuning pulse durations of $\tau \sim 5$ and 15 μs. In addition, the few sample measurements performed with $\tau = 1$ μs pulses, for which atom motion should be negligible, also fall within the data range illustrated by Fig. 2. Those data do, however, fall uniformly below the calculated curve. Thus, while atom motion may contribute slightly to the resonance widths, it does not play a substantial role in determining the width, or shape, of the resonance profiles.

A likely contributor to the resonance width discrepancy is the neglect of beyond nearest-neighbor interactions in our model. That said, the magnitude of the discrepancy indicates that these effects are probably not as large as previously indicated. The first studies of RET in a cold Rydberg gas [3,4] reported measured widths that were much (up to two orders of magnitude) broader than expected for isolated pairs of atoms. It was suggested that rapid diffusion of the population, away from an interacting nearest-neighbor pair to other nearby atoms, rapidly occurred via exchange or "hopping" interactions of the form $|P\rangle|S\rangle \rightarrow |S\rangle|P\rangle$. Subsequent experiments verified the excitation diffusion process [6,8] in the absence of other strong interactions. However, more detailed simulations [2,17] of tunable, resonant population transfer in a many-atom system showed that the primary DD coupling between nearest neighbors could suppress the diffusion process. As a result, the inclusion of exchange interactions resulted in only a modest (~50% [2]) increase in the resonance width. The amount of broadening that we observe, relative to our nearest-neighbor model, agrees with that prediction [2]. Interestingly, a similar level of resonance broadening (roughly a factor of 2 relative to the nearest-neighbor prediction) was recently observed under similar conditions, but for a much weaker DD resonance [29]. Thus, the suppression of excitation diffusion appears to be a general feature of resonantly coupled gases.

V. CONCLUSION

We have measured, as a function of atom density, the line shapes associated with $32p_{3/2}32p_{3/2} \rightarrow 32s33s$ resonant population transfer in a cold Rb Rydberg gas. The line shapes are cusplike at high density, reflecting the random nearest-neighbor separation in the MOT, and are well reproduced by closed form expressions based on a two-body interaction model. The resonance widths agree with the model up to a factor of 2, confirming that beyond nearest-neighbor processes such as excitation diffusion do not influence the population transfer rate to the degree previously indicated. At low density the change in the line shape from a cusp to Gaussian form allows us to characterize the electric field inhomogeneity in the interaction region. In the future, similar resonance line shape analyses may make it possible to distinguish random from uniform atom distributions, perhaps providing a method to visualize changes in the position correlation function with the application of controlled DD forces between atoms [15].

ACKNOWLEDGMENT

This work has been supported by the NSF.

[1] T. F. Gallagher, *Rydberg Atoms* (Cambridge University Press, Cambridge, England, 1994), and references therein.
[2] B. Sun and F. Robicheaux, Phys. Rev. A **78**, 040701(R) (2008).
[3] W. R. Anderson, J. R. Veale, and T. F. Gallagher, Phys. Rev. Lett. **80**, 249 (1998).
[4] I. Mourachko, D. Comparat, F. de Tomasi, A. Fioretti, P. Nosbaum, V. M. Akulin, and P. Pillet, Phys. Rev. Lett. **80**, 253 (1998).
[5] M. D. Lukin, M. Fleischhauer, R. Cote, L. M. Duan, D. Jaksch, J. I. Cirac, and P. Zoller, Phys. Rev. Lett. **87**, 037901 (2001).
[6] W. R. Anderson, M. P. Robinson, J. D. D. Martin, and T. F. Gallagher, Phys. Rev. A **65**, 063404 (2002).
[7] D. Tong, S. M. Farooqi, J. Stanojevic, S. Krishnan, Y. P. Zhang, R. Cote, E. E. Eyler, and P. L. Gould, Phys. Rev. Lett. **93**, 063001 (2004).
[8] I. Mourachko, W. Li, and T. F. Gallagher, Phys. Rev. A **70**, 031401(R) (2004).
[9] T. J. Carroll, K. Claringbould, A. Goodsell, M. J. Lim, and M. W. Noel, Phys. Rev. Lett. **93**, 153001 (2004).
[10] K. Singer, M. Reetz-Lamour, T. Amthor, L. G. Marcassa, and M. Weidemüller, Phys. Rev. Lett. **93**, 163001 (2004).
[11] F. Robicheaux and J. V. Hernández, Phys. Rev. A **72**, 063403 (2005).
[12] T. Cubel Liebisch, A. Reinhard, P. R. Berman, and G. Raithel, Phys. Rev. Lett. **95**, 253002 (2005).
[13] S. Westermann, T. Amthor, A. L. de Oliveira, J. Deiglmayr, M. Reetz-Lamour, and M. Weidemüller, Eur. Phys. J. D **40**, 37 (2006).
[14] T. Vogt, M. Viteau, J. Zhao, A. Chotia, D. Comparat, and P. Pillet, Phys. Rev. Lett. **97**, 083003 (2006).
[15] M. L. Wall, F. Robicheaux, and R. R. Jones, J. Phys. B **40**, 3693 (2007).
[16] C. S. E. van Ditzhuijzen, A. F. Koenderink, J. V. Hernández, F. Robicheaux, L. D. Noordam, and H. B. van Linden van den Heuvell, Phys. Rev. Lett. **100**, 243201 (2008).
[17] K. C. Younge, A. Reinhard, T. Pohl, P. R. Berman, and G. Raithel, Phys. Rev. A **79**, 043420 (2009).
[18] A. Gaëtan, Y. Miroshnychenko, T. Wilk, A. Chotia, M. Viteau, D. Comparat, P. Pillet, A. Browaeys, and P. Grangier, Nat. Phys. **5**, 115 (2009).
[19] E. Urban, T. A. Johnson, T. Henage, L. Isenhower, D. D. Yavuz, T. G. Walker, and M. Saffman, Nat. Phys. **5**, 110 (2009).
[20] R. Löw, H. Weimer, U. Krohn, R. Heidemann, V. Bendkowsky, B. Butscher, H. P. Büchler, and T. Pfau, Phys. Rev. A **80**, 033422 (2009).
[21] T. Pohl and P. R. Berman, Phys. Rev. Lett. **102**, 013004 (2009).
[22] I. I. Ryabtsev, D. B. Tretyakov, I. I. Beterov, and V. M. Entin, Phys. Rev. Lett. **104**, 073003 (2010).
[23] T. Pohl, E. Demler, and M. D. Lukin, Phys. Rev. Lett. **104**, 043002 (2010).
[24] S. Wüster, C. Ates, A. Eisfeld, and J. M. Rost, Phys. Rev. Lett. **105**, 053004 (2010).
[25] J. D. Pritchard, D. Maxwell, A. Gauguet, K. J. Weatherill, M. P. A. Jones, and C. S. Adams, Phys. Rev. Lett. **105**, 193603 (2010).
[26] A. Schwarzkopf, R. E. Sapiro, and G. Raithel, Phys. Rev. Lett. **107**, 103001 (2011).
[27] F. Bariani, Y. O. Dudin, T. A. B. Kennedy, and A. Kuzmich, Phys. Rev. Lett. **108**, 030501 (2012).
[28] M. Viteau, P. Huillery, M. G. Bason, N. Malossi, D. Ciampini, O. Morsch, E. Arimondo, D. Comparat, and P. Pillet, Phys. Rev. Lett. **109**, 053002 (2012).
[29] M. R. Kutteruf and R. R. Jones, Phys. Rev. Lett. **108**, 013001 (2012).
[30] H. Schempp, G. Gunter, M. Robert-de-Saint-Vincent, C. S. Hofmann, D. Breyel, A. Komnik, D. W. Schonleber, M. Garttner, J. Evers, S. Whitlock, and M. Weidemüller, Phys. Rev. Lett. **112**, 013002 (2014).
[31] D. Tiarks, S. Baur, K. Schneider, S. Dürr, and G. Rempe, Phys. Rev. Lett. **113**, 053602 (2014).
[32] Y. O. Dudin and A. Kuzmich, Science **336**, 887 (2012).
[33] M. Saffman, T. G. Walker, and K. Mølmer, Rev. Mod. Phys. **82**, 2313 (2010), and references therein.
[34] L. Isenhower, E. Urban, X. L. Zhang, A. T. Gill, T. Henage, T. A. Johnson, T. G. Walker, and M. Saffman, Phys. Rev. Lett. **104**, 010503 (2010).
[35] D. Paredes-Barato and C. S. Adams, Phys. Rev. Lett. **112**, 040501 (2014).
[36] M. Ebert, M. Kwon, T. G. Walker, and M. Saffman, Phys. Rev. Lett. **115**, 093601 (2015).
[37] N. Saquet, A. Cournol, J. Beugnon, J. Robert, P. Pillet, and N. Vanhaecke, Phys. Rev. Lett. **104**, 133003 (2010).
[38] M. R. Kutteruf and R. R. Jones, Phys. Rev. A **82**, 063409 (2010).
[39] M. R. Kutteruf, Ph.D. thesis, University of Virginia, 2010.
[40] P. Hertz, Math. Ann. **67**, 387 (1909).
[41] M. Abramowitz and I. Stegun, *Handbook of Mathematical Functions with Formulas, Graphs, and Mathematical Tables* (Dover Publications, New York, 1964).